scientific reports

Check for updates

OPEN

Structural analysis shows the mode of inhibition for *Staphylococcus aureus* lipase by antipsychotic penfluridol

Julia Kitadokoro[1], Takatsugu Hirokawa[2,3], Masayuki Kamo[4], Naoki Furubayashi[4], Yukiko Okuno[5], Takaaki Hikima[6], Masaki Yamamoto[6], Koji Inaka[4], Katsumi Maenaka[7,8,9,10], Shigeki Kamitani[11] & Kengo Kitadokoro[1]✉

It is now well-established that *Staphylococcus aureus* can produce a range of toxin proteins, resulting in a spectrum of pathological conditions when it infects individuals with pre-existing medical conditions or immunocompromised. Among these, MRSA is one of the most prominent antimicrobial-resistant organisms and a significant cause of mortality in many patients. It has been demonstrated that *Staphylococcus aureus* lipase (SAL) is a vital factor in the proliferation of this bacterium. A combination of *in silico* screening and X-ray crystallography was employed to analyze inhibitors of SAL, and the results were highly significant. *In silico* screening identified a number of compounds, and the enzyme activity assay demonstrated that the antipsychotic drug penfluridol exhibited potent inhibitory activity against SAL. We have conducted co-crystallization of penfluridol and SAL on the ground and in space. The resulting co-crystals were subjected to data measurement using the synchrotron radiation facility at SPring-8, and the complex structure was determined. The crystal structure of the penfluridol-SAL complex was determined at 2.2 Å resolution, thereby providing the structural basis for developing new anti-infective agents that inhibit the growth of *Staphylococcus aureus*. These findings are anticipated to facilitate the development of compounds with potent inhibitory activity.

The number of deaths attributable to antimicrobial resistance (AMR), a condition where bacteria evolve and become resistant to antimicrobial agents and antibiotics, is increasing and has become a significant global challenge[1]. It is estimated that more than 35,000 deaths occur annually in the United States, and 33,000 deaths occur annually in Europe. It is estimated that the number of deaths related to AMR worldwide could reach 10 million per year by 2050[2]. Methicillin-resistant *Staphylococcus aureus* (MRSA) is the most prevalent drug-resistant organism responsible for nosocomial and community-acquired infections[3,4].

Staphylococcus aureus is a facultative anaerobic gram-positive bacillus[5]. It is in high numbers on humans' and animals' skin, nasal passages, and other body surfaces[6]. The yellowish nasal discharge commonly observed during a cold is a consequence of the pigmentation of this bacterium. It is widely distributed in nature and can be isolated ex vivo from air, soil, and dairy products. It is most prevalent in the crusts of wounds. *S. aureus* produces a multitude of toxin proteins that can result in a wide range of severe infections, including soft tissue

[1]Faculty of Molecular Chemistry and Engineering, Graduate School of Science and Technology, Kyoto Institute of Technology, Hashigami-cho, Matsugasaki, Sakyo-ku, Kyoto 606-8585, Japan. [2]Transborder Medical Research Center, University of Tsukuba, Tsukuba, Ibaraki 305-8575, Japan. [3]Division of Biomedical Science, Faculty of Medicine, University of Tsukuba, Tsukuba, Ibaraki 305-8575, Japan. [4]MARUWA Foods and Biosciences, Inc., 170-1, Tsutsui-cho, Yamatokoriyama, Nara 639-1123, Japan. [5]Medical Research Support Center, Graduate School of Medicine, Kyoto University, Yoshidakonoe, Sakyo-ku, Kyoto 606-8501, Japan. [6]SR Life Science Instrumentation Team, Life Science Research Infrastructure Group, Advanced Photon Technology Division, RIKEN SPring-8 Center, 1-1-1, Koto, Sayo-cho, Sayo-gun, Hyogo 679-6148, Japan. [7]Laboratory of Biomolecular Science, and Center for Research and Education on Drug Discovery, Faculty of Pharmaceutical Sciences, Hokkaido University, Sapporo, Hokkaido 060-0812, Japan. [8]Division of Pathogen Structure, International Institute for Zoonosis Control, Hokkaido University, Sapporo 001-0020, Japan. [9]Global Station for Biosurfaces and Drug Discovery, Hokkaido University, Sapporo, Hokkaido 060-0812, Japan. [10]Institute for Vaccine Research and Development (HU-IVReD), Hokkaido University, Sapporoo, Hokkaid 060-0812, Japan. [11]Department of Nutrition, Graduate School of Human Life and Ecology, Osaka Metropolitan University, 3-7-30 Habikino, Habikino, Osaka 583-8555, Japan. ✉email: kengo@kit.ac.jp

infections such as pyogenesis, impetigo, folliculitis, and abscesses, as well as pneumonia, peritonitis, sepsis, and meningitis[7,8]. Moreover, it is a causative agent of food poisoning, toxic shock syndrome, and enteritis[8]. The organism is known to cause pneumonia, septicemia, and other severe infections in individuals with underlying diseases, such as the elderly, the sick, and young children with weakened immune systems[9].

It is well documented that *Staphylococcus aureus* plays a role in enhancing antibiotic resistance through the formation of biofilms and persisters[10,11]. Consequently, this bacterium is attracting increasing attention worldwide as a significant pathogen responsible for opportunistic human infections. Nevertheless, a shortage of efficacious antimicrobial agents is currently available for clinical practice. In this study, we concentrated on SAL (*S. aureus* lipase). This enzyme has attracted considerable attention as a potential target for research due to its involvement in the growth of *S. aureus*[12,13].

In light of the established correlation between SAL and the proliferation of *S. aureus,* it is postulated that the inhibition of this enzyme may impede the growth of the bacteria[13]. SAL is a protein with a molecular weight of 45.7 kilodaltons secreted as an enzyme consisting of 394 amino acid residues[12]. Glycerol ester hydrolase (Geh) is an enzyme that catalyzes the hydrolysis of triacylglycerol, a common lipid component. Its enzymatic function is based on the typical catalytic triad, comprising serine, aspartate, histidine residues, and oxyanion holes, which are analogous to those observed in serine proteases[12].

The three-dimensional structure of SAL has already been determined, and the detailed structural mode of the inhibitor orlistat has been elucidated[14]. Orlistat is an anti-obesity pharmaceutical agent that inhibits the activity of gastric and pancreatic lipases[15]. Moreover, it has been demonstrated to exert inhibitory activity against SAL[14]. The detailed structural information was utilized in an *in silico* screening process to identify potential inhibitors of existing drugs.

In silico screening represents an effective methodology for identifying efficacious inhibitors within compound databases[16]. When crystal structures of enzyme-inhibitor complexes are available, docking studies employing programs such as *Glide* can rapidly identify potential compound candidates[17,18]. Nevertheless, the probability of successful drug design remains low, with a 2–3% correct response rate to identify compounds of the µmol order for which IC_{50} can be calculated.

The drug repositioning process, which encompasses *in silico* screening and repurposing of existing pharmaceuticals, has been attempted on numerous occasions in search of therapeutic agents that can effectively combat COVID-19 coronaviruses[19]. Given the substantial financial investment and extended approval timeline associated with the discovery and development of new drugs, repurposing existing, previously approved pharmaceuticals is becoming an increasingly appealing strategy[20,21]. This is because it entails reduced overall development costs, shorter development times, and the utilization of less risky compounds, which collectively contribute to a more efficient and cost-effective drug development process. The potential of drug repurposing (also known as drug repositioning) has been demonstrated; anti-obesity drugs, for instance, have been shown to exhibit inhibitory activity in SAL[14].

In silico techniques have been employed in conjunction with databases such as KEGG to identify potential drug candidates for repurposing[22,23]. We were fortunate to identify an inhibitor among the 13 compounds obtained through *in silico* methods, which exhibited potent inhibitory activity (Supplemental Fig. S1). The compound in question is penfluridol, which has a long history of use as an antipsychotic (Fig. 1a)[24].

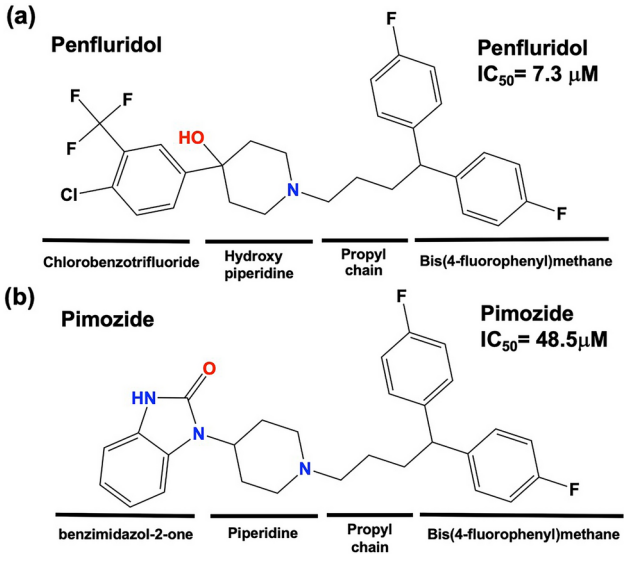

Fig. 1. Chemical structures of Penfluridol and Pimozide, with IC_{50} values. Relative activities were measured at different inhibitor concentrations. The two compounds exhibited a striking resemblance in their skeletal structures, with the sole distinction lying in the leftmost group depicted in the figure, which ultimately manifested in disparate solubility characteristics.

Penfluridol is a highly potent first-generation diphenylbutylpiperidine antipsychotic that has been demonstrated to suppress the imbalance in the inflammatory response in LPS-induced macrophages by inhibiting the activation of the NLRP3 inflammasome[25]. It is a drug that is widely utilized in clinical practice.

Penfluridol is a relatively large compound comprising a biphenyl moiety with two benzene fluorides, a central heterocyclic ring system (comprising piperazine and piperidine groups) containing at least one nitrogen atom, which forms the backbone of the compound, and a benzene ring with a trifluoromethyl group and a chloro group attached to it, with three carbon atoms (Fig. 1a). As illustrated in Fig. 1a, three carbon chains link the two units.

One hundred compounds were selected for *in silico* screening through molecular docking calculations using the *Glide* program against 49,000 existing drug compounds in the KEGG database (Fig. S1)[17,18,22,23].The results demonstrated that penfluridol exhibited potent inhibitory activity. This study had two objectives: first, to calculate the IC_{50} of penfluridol, which shows inhibitory activity against SAL, and second, to obtain a detailed structure with higher resolution and precision by attempting to crystallize the complex of SAL and penfluridol on Earth and under weightless conditions with the assistance of JAXA. For penfluridol, which demonstrated robust inhibitory activity, the half-inhibition constant (IC_{50}) was calculated, and the complex of SAL and penfluridol was co-crystallized.

X-ray diffraction data for crystals of the SAL complexed with inhibitors were collected at the SPring-8 beamlines BL41XU and BL44XU. The structures were determined by the molecular replacement method, and molecular models were constructed from the obtained electron density maps to determine the steric structures of SAL and the existing drug Penfluridol.

Results

In silico screening and IC_{50} measurement by activity assay

In silico screening using *Glide* selected 100 compounds from the existing KEGG drug database[22,23]. The interaction between SAL and orlistat was analyzed using the coordinates of the structure of the complex of SAL and orlistat (pdbid: 6KSM). Consequently, a range of active site regions of SAL involved in binding to the inhibitor was selected, and the distribution of amino acids within these regions was verified. Furthermore, the electron donor, electron acceptor, and hydrophobic portions were determined on *Glide*, and compounds from the KEGG database that fit into the active site of SAL in terms of both inhibitor shape and electron distribution were selected. The selection of these 100 compounds was based on the Glidescore docking score value, which was utilized as an indicator. Compounds with Glidescore scores ranging from − 10 to − 8.6 were included in the list. Subsequently, the inhibitory activity of these compounds was validated sequentially, commencing with the most prioritized compounds (Fig. S1). As previously reported, the activity of the compounds was quantified by measuring the absorption wavelength at 405 nm of para-nitrophenol produced by the degradation of *p*-nitrophenyl butyrate (*p*NPB)[14]. A series of inhibitor solutions, with concentrations ranging from 1 to 100 mM, were added to cuvettes containing SAL, buffer, and water solutions. Subsequently, the alterations in absorbance were quantified by introducing a *p*NPB substrate solution dissolved in DMSO into the cuvettes. The initial absorbance was then measured over time and compared to the uninhibited solution's slope to calculate the inhibition percentage.

Among the selected inhibitors, penfluridol, a dopamine receptor inhibitor, was identified as a SAL inhibitor, with an IC_{50} value of 7.3 μM (Figs. 1a, 2a). Penfluridol is a first-generation diphenylbutylpiperidine antipsychotic with potent antipsychotic activity. The IC_{50} values were found to be as potent as those of previously identified inhibitory compounds, including orlistat (IC_{50} = 2.4 μM) Petroselinic acid (IC_{50} = 3.4 μM) and Farnesol (IC_{50} = 570 μM) (Fig. S2)[13,14,26].

X-ray structure analysis of SAL-penfluridol complex

Furthermore, co-crystals of the SAL-penfluridol complex were prepared. The solubility of penfluridol was found to be high, with the highest solubility observed in DMSO at 100 mg/mL. It was determined to be a suitable inhibitor of the co-crystallization process (see Fig. S1). The crystallization conditions were 2.8–3.01 M sodium formate and 0.1 M acetate buffer at pH 6.5, maintained at 295 K. The crystallization conditions were similar to those previously reported and yielded reproducible, diamond-shaped crystals in approximately one to two weeks[14,26].

Penfluridol was the third Glidescore among the compounds that were available, and the higher scoring compounds Indacaterol (adrenergic β2 receptor agonist)[27] and Olaparib (PARP inhibitor; for the treatment of breast and ovarian cancer)[28] had lower solubility and were co-crystallized for data measurement (Fig. S1). The 2.41 Å resolution for Indacaterol (accompanied by six additional data sets) and the 2.19 Å resolution (along with 35 other data sets) were measured for Olaparib. The analysis revealed no binding at all, and since the crystal structure did not show binding of the inhibitor, the exact IC_{50} was not determined.

Moreover, the co-crystallization of the SAL-penfluridol complex was conducted at 293 K in a microgravity environment. In Projects MT8 and MT9, crystallization in microgravity conditions was successfully achieved in the thermostatic chamber of the Kibo Pressurized Module (PM) using a counter-diffusion method, resulting in the formation of highly pure hexagonal crystals (Fig. S3)[29].

The data measurements of these composite crystals were conducted at BL41XU and BL44XU at SPring-8, and the resulting data exhibited a resolution of approximately 2.23 Å (on the ground, PDBid: 9L3C) and 2.57 Å (in space, PDBid: 9L3S), respectively. The SAL- penfluridol crystal (on the ground) was found to have space group $P4_122$, with lattice constants $a = b = 127.5$ and $c = 252.5$ Å. It was nearly isomorphic to the native crystal, containing two molecules in the asymmetric unit (see Table 1)[14]. The structures were determined by the molecular replacement method using *Phaser* in *CCP4* for structural analysis, and molecular modeling was performed in *Coot*[30–32]. The results of the molecular replacement analysis indicated the presence of an electron

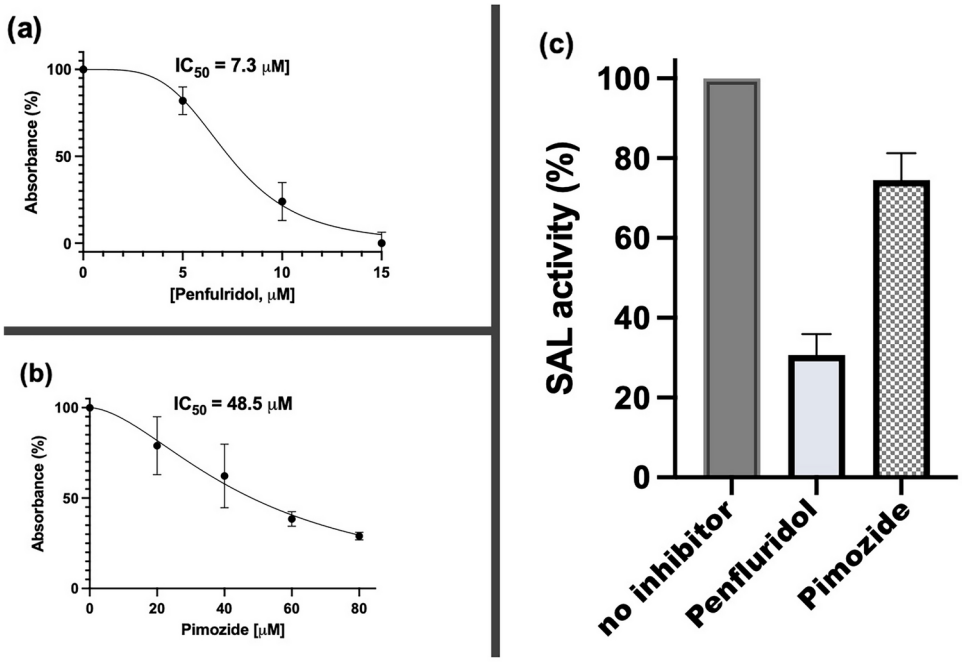

Fig. 2. Inhibition of SAL by Penfluridol and Pimozide. The IC_{50} value was determined using the IC_{50} calculator (https://www.aatbio.com/tools/ic50-calculator). SAL activity towards *p*-nitrophenylbutyrate. Enzymatic activity was measured by monitoring *p*-nitrophenol production. Each data point is presented as mean ± SEM with error bars representing SEM (n = 3). (**a**) The IC_{50} of Penfluridol versus SAL. (**b**) The IC_{50} of Pimozide versus SAL. (**c**) Comparison of increased SAL activity of the same concentrations of Penfluridol and Pimozide. (20 μM each). Values without inhibitors are taken as 100%. The statistical software used was Prism9 (GraphPad), with one-way ANOVA tests and Dunnet for multiple comparisons.

density near the active site in both the ground and space crystals, which appeared to be penfluridol (Fig. 3a, b). The active site's electron density was highly reproducible (Fig. 3a, b).

Coot's Ligand Builder was employed to fit a model molecule of penfluridol to the electron density[32], and the structure of SAL and penfluridol was successfully determined through a process of repeated structure refinement analysis conducted using the *Refmac* software[33].

Structural refinement resulted in the determination of a stereochemically correct structure with an R*factor* value of 20.2% and an R*free* value of 23.1%, indicating the certainty of the structure, using data at 2.23 Å resolution (Table 1).

Structure of the SAL-penfluridol complex

The monomeric structure of SAL exhibited similarity to that reported in previous studies and retained the typical α/β-hydrolase structure, consisting of 13 β-strands, 13 α-helices, and six 3_{10}-helices (Fig. 4)[14,26]. The SAL exhibited the characteristic of two large hydrophobic pockets extending from the active center, Ser116[14], as observed in previous studies (Figs. 4, 5). The nucleophilic atom Ser116 was identified within the so-called "β-elbow" loop, situated between the β-chain and α-helix of the α/β hydrolase center[34]. Like other serine hydrolases, it contains three catalytic triad residues, namely His349, Asp307, and Ser116, which are essential for the catalytic mechanism. The nitrogen atoms in the leading chains of Phe17 and Met117 form oxyanion holes, which can serve to stabilize intermediate transition states during the reaction[14,26].

The SAL-penfluridol complex was also a dimeric molecule with one molecule of penfluridol bound to each of the A and B chains, and the binding mode of the two penfluridol molecules to SAL was identical (Fig. 5).

The electron density was observed to be reproducible at the active site (Fig. 3). The success of this complex analysis may be attributed, at least in part, to the high solubility of penfluridol. In comparison with the native crystal resolution of 2.0 Å, the penfluoridol complex crystal reflection exhibited relative weakness, yielding only approximately 2.5–2.7 Å. In this study, the highest resolution data of 2.23 Å was obtained. The acquisition of high-resolution data was facilitated by circumventing the conventional approach of making 180-degree measurements on single crystals, making 360-degree measurements, and integrating only those data deemed to be of sufficient quality. Structural analysis was also performed for all other 12 compounds, but due to the solubility of the inhibitors, precipitation often occurred, and complex structures could not be obtained (Fig. S1). Further activity assays showed that 12 species, other than penfluridol, had little or no inhibitory activity (Supplementary Fig. S1).

	SAL/Penfluridol complex on the ground	SAL/Penfluridol complex in space
PDB ID	9L3C	9L3S
Diffraction source	BL41XU/SPring-8	BL44XU/SPring-8
Wavelength (Å)	0.9	0.9
Temperature (K)	100	100
Detector	Eiger X 16 M	Eiger X 16 M
Crystal–detector distance (mm)	240	300
Rotation range per image (°)	0.1	0.1
Total rotation range (°)	360	180
Exposure time per image (s)	0.1	0.1
Space group	$P4_122$	$P4_122$
a, *b*, *c* (Å)	127.5 127.5, 252.5	127.3 127.3, 255.4
α, *β*, *γ* (°)	90.0, 90.0, 90.0	90.0, 90.0, 90.0
Mosaicity (°)	0.160	0.126
Resolution range (Å)	50–2.23 (2.37–2.23)	50–2.57 (2.72–2.57)
Total no. of reflections	2,524,098	899,897
No. of unique reflections	192,595	126,877
Completeness (%)	99.8 (98.7)	99.8 (98.7)
Redundancy	13.1 (13.0)	7.1 (7.1)
$\langle I/\sigma(I)\rangle$	12.4 (0.5)	11.0 (0.5)
R_{meas}	0.164 (3.603)	0.113 (3.496)
$CC_{1/2}$	0.998 (0.457)	0.999 (0.396)
Refinement	*Refmac*	*Refmac*
Resolution range (Å)	50–2.23	50–2.57
R-factor/free *R*-factor (%)	19.0/22.4	19.8/22.7
No. of atoms	6327	6277
No. of solvent atoms	46	8
Ramachandran distribution (% favored, allowed, outlier)	98.7, 1.3, 0	97.6, 2.4, 0
RMS bonds (Å), angles (°)	0.008, 1.57	0.006, 1.64
Average B value ($Å^2$)	74.6	75.0

Table 1. Data collection, processing, and refinement. Outer shell values are shown in parentheses. Completeness for all reflections and the highest resolution shell in parentheses. Completeness for all reflections and the highest resolution shell in parentheses.

Interaction of SAL-penfluridol complex

The figure shows an enlarged view of the SAL-penfluridol complex in the vicinity of the active site (Fig. 3a, b). The structure of penfluridol was Y-shaped (Figs. 3, 4, 5, 6 and 7). Two fluorophenyls spread their hands, and the remaining residue extended from the junction. The IUPAC nomenclature for penfluridol is 1-[4,4-bis(4-fluorophenyl)butyl]-4-[4-chloro-3-(trifluoromethyl)phenyl]piperidin-4-ol, which is composed of four distinct parts (Fig. 1a). In other words, the molecule consists of a trifluoromethyl phenyl chloride group, a piperidine ring, and three alkyl chains that serve as linkers, followed by two fluorinated phenyl groups (Fig. 1a).

The binding mode of penfluridol differs from previous results, as evidenced by the interaction of the two phenyl fluoride rings across the hydrophobic pocket, which slightly widens the pocket (Fig. 7a, b)[14,26]. No direct covalent binding to the active residue, Ser116, was observed. The electron density map showed that Ser116 was involved in a binding interaction with the formic acid molecule in the crystallization reagent. The formic acid molecule was then placed in the so-called oxyanion hole, consisting of nitrogen atoms in the main chains of Phe17 and Met117, stabilizing the binding state of SAL and penfluridol. In addition, another molecule of formic acid B was present close to formic acid A (Figs. 3a, b, 6). This formic acid B interacted with the piperazine ring of penfluridol and also interacted with formic acid A, thereby mediating the bond between Ser116 and penfluridol (Figs. 3a, b, 6). The mode of bonding exhibited a high degree of similarity between the terrestrial and extraterrestrial environments. A similar phenomenon was observed with the alkyl chains that followed the biphenyl chain, where the electron density was thinner.

Indeed, SALs with excess penfluridol were removed by the Econo-Pac 10DG column, and their activity was found to be minimal, as shown in the Supplementary Data (Fig. S4ab). This suggests that the inhibitors may be covalently bound to the SAL. The data suggest that the inhibition is covalently bound in a manner distinct from the binding of the active site to Ser116.

The inhibition mechanism of this compound was found to be novel in that it does not involve direct covalent binding to the active residue Ser116. Alternatively, the active residue Ser116 interacts with the formic acid used

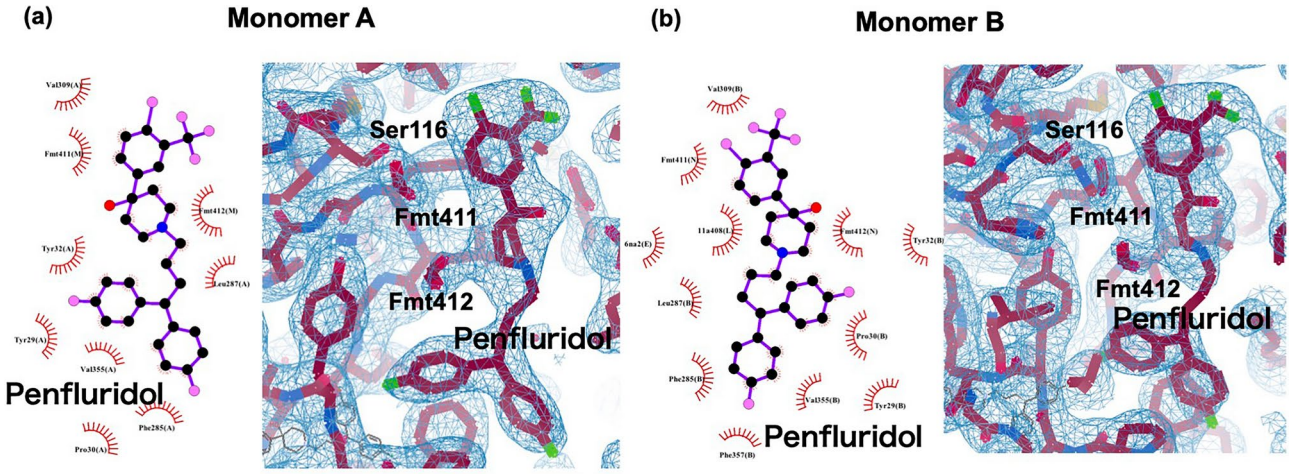

Fig. 3. (**a**) The primary interactions of penfluridol within the active site of the A chain of SAL are depicted using the *LIGPLOT*+ diagram on the right[42] and the electron density diagram on the left (The 2Fo-Fc electron density map calculated at 1.0 sigma). (**b**) A. The primary interactions of penfluridol within the active site of the B chain of SAL are depicted in the *LIGPLOT*+ diagram on the right[42] and the electron density diagram on the left. Fmt indicates formic acid.

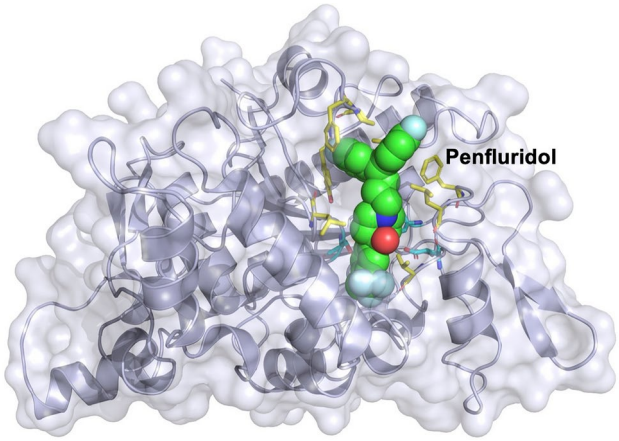

Fig. 4. The figure depicts the crystal structure of the monomer of the SAL-perfurylidol complex, with a ribbon model of the SAL structure and a fine decapod model. A sphere represents the penfluridol molecule. The residues involved in the interaction are indicated by yellow sticks. The fluorine atoms are illustrated as cyanide spheres. All molecular structure images were obtained from *PyMOL* (http://www.pymol.org/).

for crystallization and binds to trifluoromethyl phenyl chloride via formic acid (Figs. 3a, b, 6). It is conceivable that water molecules, rather than formic acid, facilitate binding in solution.

The trifluoromethyl group was observed to interact with Ala174, Ala175, and Phe17 and Phe178. The chloro group was close to Leu242 (Figs. 3a, b, 6). The phenyl ring was located between Phe17 and Val309. The piperidine ring connected to the phenyl ring was located between Leu18 and Met288, where an electron density was observed that could be attributed to either water or formic acid (Fig. 3a, b). The alkyl chain connecting the piperidine ring to the two fluorophenyl rings exhibited a slightly lower density, with a clear electron density observed in the A chain and a slightly disconnected disorder in the B chain (Fig. 3a, b).

One of the biphenyl fluorides was observed to form hydrophobic interactions with a phenylalanine cluster consisting of three phenylalanine residues (Phe285, Phe286, Phe357) and Leu287 at the active site (Fig. 6). The second phenyl fluoride was captured by a hydrophobic scissors cluster consisting of Tyr29 and Pro30 and further interacted with a hydrophobic cluster of Tyr32, Val350, Ile353, and Val355 (Fig. 6).

The results of this analysis were comparable to those of the *in silico* analysis, although there were some discrepancies in the structural data (Fig. 8a, b). Notably, the predicted positions of the trifluoromethyl group and the chlorine moiety were reversed from left to right (Fig. 8a, b). In the prediction, the trifluoromethyl group was observed to be close to Ser116 (Fig. 8b). In addition, minor discrepancies were observed in the positions of the two fluorophenyl rings, with the hydrophobic residues surrounding these rings being shifted to expand the hydrophobic pocket (Fig. 7a, b).

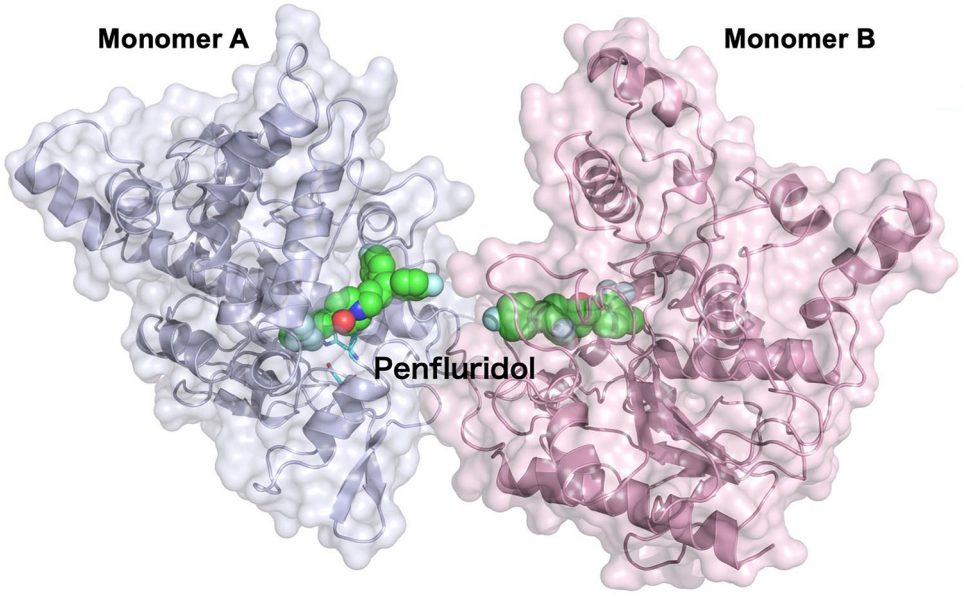

Fig. 5. The figure depicts the SAL dimer and penfluridol complexes. The monomers are illustrated in blue (chain A) and pink (chain B), and penfluridol bound to the A and B molecules is depicted as a green sphere. The packing between monomers exhibited the same symmetry as the complex structure that had been previously analyzed[14,26].

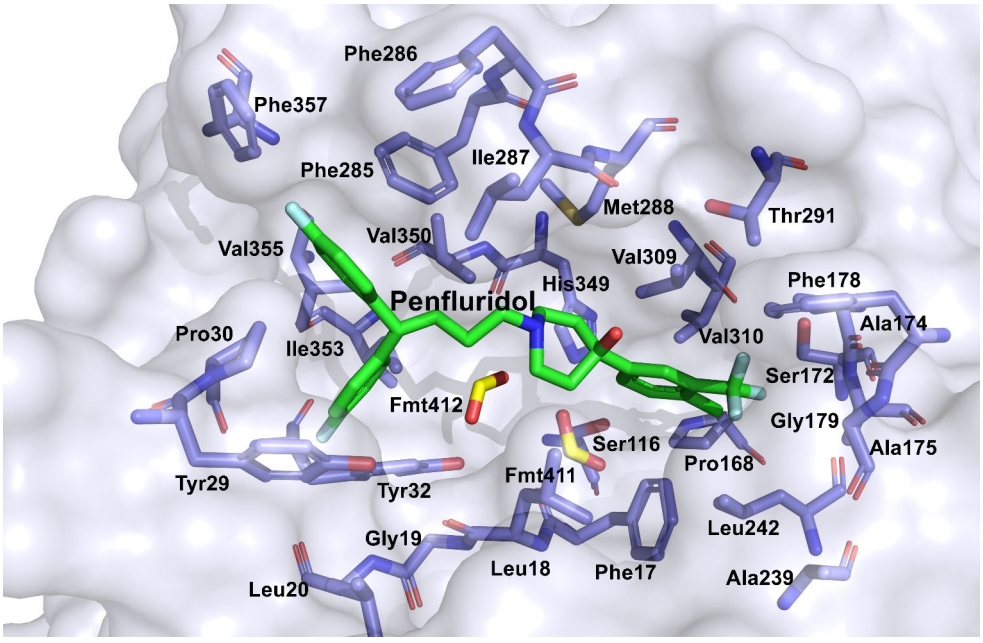

Fig. 6. The interaction of penfluridol with amino acid residues at the catalytic site of SAL is illustrated. Blue sticks indicate the residues involved in binding. For penfluridol, carbon is drawn in green, oxygen in red, nitrogen in blue, and fluorine and chlorine in pale blue. The two formate ions are written in yellow. For further details, please refer to the accompanying text.

Fluorescence changes due to the interaction of penfluridol and SAL

The relationship between SAL and penfluridol was further investigated using data from previous studies and fluorescence measurements. A recent study conducted by a research group in China showed that penfluridol inhibited *S. aureus* growth in a concentration-dependent manner[35]. However, it is important to note that this study did not investigate the involvement of SAL[35].

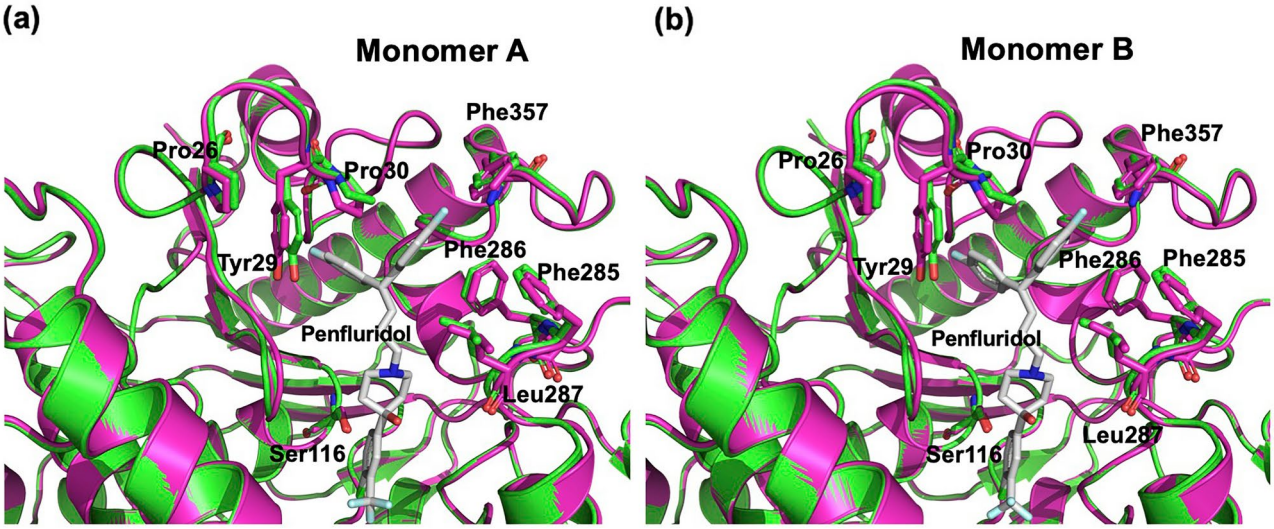

Fig. 7. The superimposition of structures around the active site was conducted with wild-type SAL and SAL-Penfluridol complex structures as monomers. The representation of penfluoridol bound to the A and B molecules is illustrated by sticks, with oxygen depicted in red, nitrogen in blue, chlorine in green, and fluorine in light blue. In **a**, wild-type SAL and complex A molecules are shown in green and magenta, respectively. The amino acid residues in the vicinity of the biphenyl moiety, which has undergone numerous structural changes, are indicated by stick notation. In **b**, wild-type SAL and B molecules of the complex are also shown in green and magenta, respectively.

The supplementary Fig. S5a shows the fluorescence spectrum of penfluridol, which shows a concentration-dependent change in the fluorescence spectrum of SAL (Fig. S5a). Specifically, an increase in the concentration of SAL resulted in a shift to a lower wavelength (435 nm) in the fluorescence spectrum (Supplementary Fig. S5a). The observed relationship between penfluridol and growth inhibition suggests that this compound may be a potential diagnostic agent for detecting *S. aureus.* This would facilitate the rapid detection of *S. aureus*.

After studying the shift in the fluorescence wavelength peak, it was proposed that the effect of fluorescence resulting from the rotation of the benzene fluoride ring may have been modified by binding to the active site of SAL (Fig. S5b). It was postulated that the intramolecular motion of penfluridol, capable of rotation, would be inhibited by binding to the active site of SAL (Fig. S5b). This would result in suppressing the rotation of the benzene difluoride of penfluridol, which would lead to a change in fluorescence (Fig. S5ab). Indeed, the electron density was also slightly reduced in the region of the carbon chain, leading to the two benzene difluorides (Fig. 3a, b), which we interpreted as an indication of the magnitude of the intramolecular fluctuations.

Discussion

Penfluridol was identified as a promising candidate compound in the *in silico* screening process and was ranked 15th (Fig. S1). Pimozide, a compound with structural similarity to penfluridol, was the 84th compound to undergo evaluation in the *in silico* screening process (Fig. S1). Pimozide is a neuroleptic drug indicated primarily for the treatment of schizophrenia[36]. Furthermore, it has been utilized in treating autism in pediatric patients. The IC_{50} value of this drug, which has a similar structure to that of penfluridol, was determined. Moreover, an attempt was made to determine the structure of the complex. The IC_{50} of pimozide was determined to be approximately 48.5 μM (Fig. 2b). The value for penfluridol was 7.3 μM, indicating that penfluridol is approximately six times more potent in inhibitory activity than pimozide (Fig. 2c). A comparison of the structural formulas for these compounds is presented in Fig. 1. The IUPAC names for penfluridol and pimozide are 1-[4,4-bis(4-fluorophenyl)butyl]-4-[4-chloro-3-(trifluoromethyl)phenyl]piperidin-4-ol and 3-[1-[4,4-bis(4-fluorophenyl)butyl]piperidin-4-yl]-1H-benzimidazol-2-one, respectively. The structural similarity between the biphenyl fluoride and piperazine groups and the propyl chain moieties linking them, with a terminal methyl trifluoride group, is responsible for the fivefold difference in activity between pimozide and benzimidazole (Figs. 1a, b, 2a–c)[36]. The compound with the structure of diphenylbutylpiperidine is a prototypical antipsychotic drug (Fig. 1a, b).

In all 11 diffraction data sets of SAL-pimozide co-crystals measured at SPring-8, no evidence of pimozide binding to the pimozide-SAL complex crystal was observed. This was attributed to the low solubility and low inhibitory activity of pimozide (Fig. S1). In stark contrast to pimozide, which displayed markedly low solubility (Solubility of 18 mg/mL in DMSO)[36], penfluridol exhibited markedly high aqueous solubility (100 mg/mL in DMSO) (Fig. S1). Due to its high solubility and pronounced inhibitory effect, the electron density of penfluridol was distinctly discernible (Fig. 3a, b), whereas no map was discernible for pimozide.

The results demonstrate that both the fluorinated biphenyl moiety and the terminal substituents substantially influence the binding of SAL to penfluridol. The predicted binding mode of pimozide was arranged such that the oxygen molecule of the carbonyl group of the terminal benzimidazole was observed to bind to the active

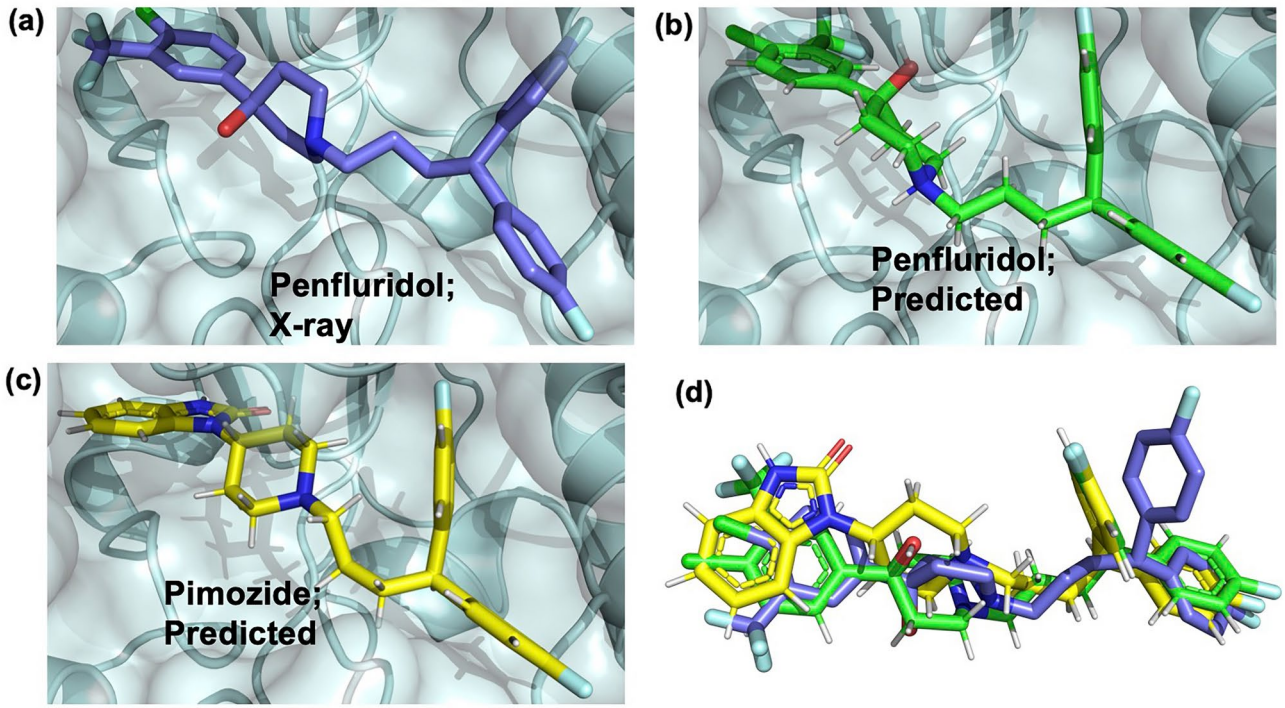

Fig. 8. The position of the inhibitor penfluridol within the complex structure is illustrated. (**a**) The blue sticks represent the results of the X-ray analysis. (**b**) The green molecule represents the predicted binding mode of penfluridol, as calculated by the *Glide* program. The chlorobenzotrifluoride group on the left has been relocated from its original position to the right in accordance with the findings of the X-ray analysis. The molecule is depicted as a green stick, and the hydrogen molecule is represented in white. (**c**) A similar approach was employed to predict the bonding diagram of the pimozide molecule. Similarly, the yellow sticks illustrate the predicted bonding diagram of the pimozide molecule. (**d**) The two molecules, resulting from the structure prediction and the X-ray analysis, are superimposed. One of the biphenyls exhibits a slight variation in the distribution of the phenyl group, while the other displays a comparable variation in the distribution of the biphenyl group.

site, Ser116 (Fig. 8c). Nevertheless, the structure could not be undetermined. Similarly, the prediction for this moiety differed from the actual experimental data for penfluridol (Fig. 8a, b). In the prediction, the methyl trifluoride group was oriented toward Ser116 (Fig. 8). However, in the actual experimental data, this orientation was reversed (Fig. 8a, b). The electron density map indicated that the orientations were, in fact, opposite one another (Fig. 3a, b).

The authors identified penfluridol as a potential inhibitor of SAL among existing pharmaceutical agents. Concurrently, a Chinese research team employed a comparable drug repositioning strategy and identified a compound that demonstrated inhibitory activity against the growth of *Staphylococcus aureus* among existing pharmaceuticals[35]. Notably, this compound was penfluridol[35]. Penfluridol demonstrated potent bactericidal efficacy against *S. aureus*, with reported minimum inhibitory concentrations (MIC) ranging between 4 and 8 μg/ml and minimum bactericidal concentrations (MBC) from 16 to 32 μg/ml[35]. Furthermore, the study revealed that penfluridol significantly impeded the formation of *Staphylococcus aureus* biofilms, with dose-dependent efficacy and the capacity to eradicate biofilms formed before 24 h[35].

The findings indicated that penfluridol was efficacious in eradicating biofilms formed within 24 h[35]. Moreover, penfluridol effectively eradicates methicillin-resistant *S. aureus* (MRSA) persistent cells in both *in vitro* and *in vivo*[35]. In particular, it demonstrated significant efficacy in mouse models of subcutaneous abscess, skin wound infection, and acute peritonitis caused by MRSA[35].

Prior research has indicated that farnesol, a terpenoid organic compound belonging to the class of linear sesquiterpenes (Fig. S2c), displays inhibitory activity against the growth of *S. aureus*[13]. The introduction of increasing quantities of farnesol was observed to result in a corresponding inhibition of bacterial growth[13]. Compared to farnesol, penfluridol demonstrated a more pronounced inhibitory effect against SAL (Fig. S2d), and a more pronounced inhibitory effect on bacterial growth[13]. This indicates that penfluridol may impede the proliferation of *S. aureus* by inhibiting SAL. These findings suggest that SAL inhibitors may have therapeutic potential as agents to prevent the growth of *S. aureus*.

Finally, the potential for SAL inhibitors with increased efficacy and reduced side effects is discussed. With regard to penfluridol, its pronounced toxicity in mouse models was considered to be a significant impediment to its practical application. Therefore, it is imperative to modify this compound's structure to ensure its safety. In this regard, we have explored the potential of a compound that exhibits enhanced selectivity in binding to the SAL.

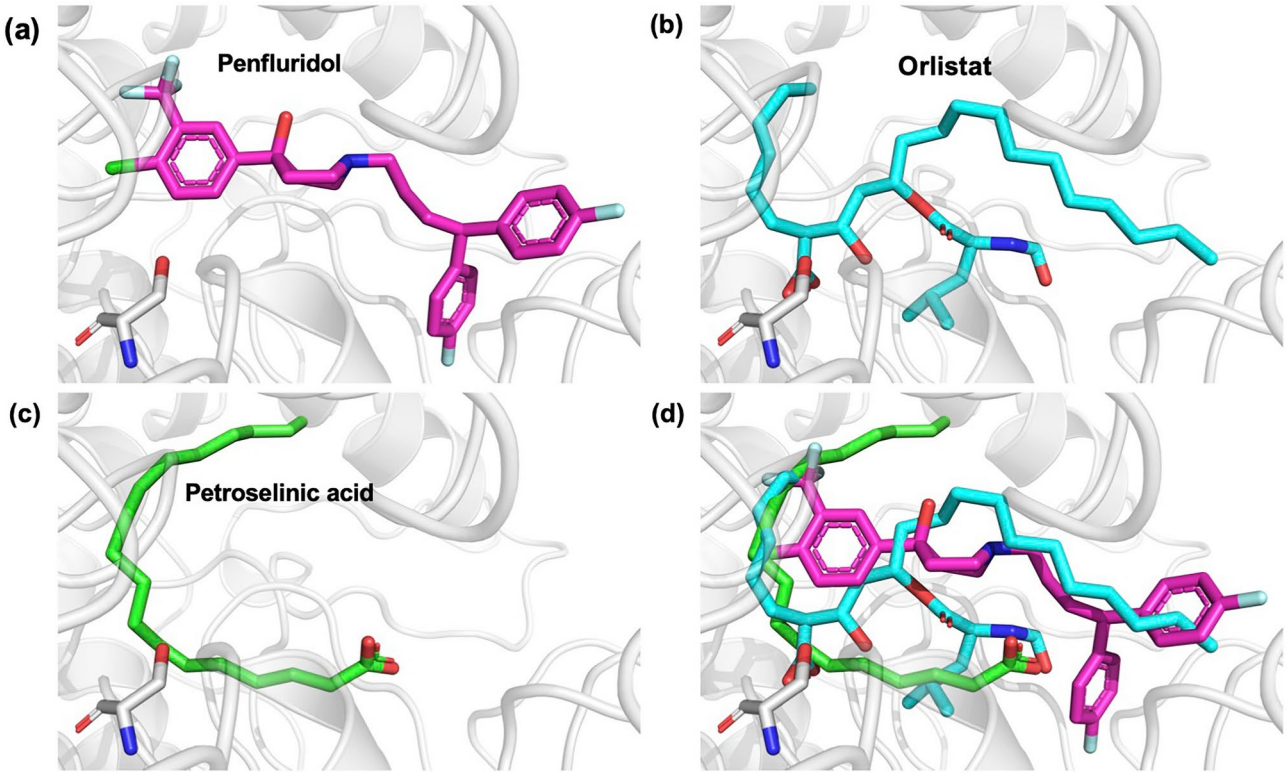

Fig. 9. A comparison was made between the SAL and the inhibitor that has been previously analyzed, using a structure overlay technique. (**a**) The structure of SAL and penfluridol is shown here. The catalytic residue Ser116 is marked with a white stick, and it is evident that it is not directly bound to penfluridol. The representation of penfluridol is indicated by magenta, oxygen by red, nitrogen by blue, chlorine by green, and fluorine by pale blue. (**b**) The structure of the SAL-Orlistat complex is illustrated, with Orlistat represented by sticks and colored cyan. Ser116 has been demonstrated to bind with Orlistat. (**c**) SAL and petroselinic acid complex structure. The green stick indicates petroselinic acid binding to Ser116. (**d**) The figure below presents a schematic representation of all inhibitors, superimposed on the binding sites of SAL.

The results of the analysis of the penfluridol complex were compared with those of the orlistat and petroselinic acid complexes that were previously analyzed and determined (Fig. 9). As illustrated by the structural formula, both orlistat and petroselinic acid consist exclusively of extended alkyl chains and are covalently bound to the active catalytic residue Ser116 (Fig. S2ab)[14, 26]. In addition, the IC_{50} values exhibited slightly greater potency in comparison to penfluridol (Fig. S2d).

In contrast, the binding mode of penfluridol was entirely distinct, exhibiting no covalent bond with Ser116 and no alkyl chain (Fig. 9a). The long alkyl chains of orlistat exhibited significant overlap with the central skeletal portion of penfluridol (Fig. 9b, d). Conversely, there was minimal overlap with the alkyl chain portion of petroselinic acid (Fig. 9c, d). In the case of orlistat, the lactone ring moiety exhibited a reaction with and binding to Ser116, while in petroselinic acid, the double bond moiety and Ser116 were covalently linked (Fig. 9b, c)[14, 26].

A novel drug design concept would be to create compounds that extend the alkyl chain from the chloro portion of the chlorobenzotrifluoride portion of penfluridol (Fig. 1a) or react with a lactone ring (Fig. 9, S2a). The creation of such compounds, if feasible, is anticipated to result in inhibitors of SAL that exhibit high selectivity and non-toxicity. The findings of this study suggest the feasibility of producing inhibitors of SAL that are both highly selective and non-toxic.

Methods

In silico analysis

The docking method was employed with the *Glide* program, based on the structural information of the SAL and orlistat complexes from a previous study[14,17,18]. The compounds were fitted against a scaffold that quantified the shape of the enzyme's active site and whether it donates or accepts charge, thereby identifying the compounds with the best binding states. From a database comprising tens of thousands of compounds, binding prediction scores were calculated, and candidate inhibitors were evaluated through enzyme-compound docking studies. The top 100 inhibitor candidates were obtained from a 49,000 existing drug compounds database in the Kyoto Encyclopedia of Genes and Genomes (KEGG)[22,23].

Expression and purification of *pColdII-SAL*

The glycerol stock containing the recombinant SAL gene in the *E. coli pColdII* vector harbored by BL21(DE3) was precultured in 50 mL LB medium containing 50 μg/mL ampicillin at 37 °C in 200 mL Meyer flasks, as previously described[14,26,37]. Ten milliliters of the preculture solution were transferred to one liter of LB medium containing ampicillin and incubated at 37 °C for approximately two hours. Subsequently, protein expression was induced by adding 0.1 mM IPTG at a final concentration. The mixture was incubated at 15 °C for 24 h. Subsequently, the cells were collected by centrifugation at 277 K for 30 min at 4000 rpm, as previously reported. The supernatant fluid was washed twice with TE buffer and suspended in lysis buffer (50 mM phosphate buffer at pH 8.0 containing 0.3 M NaCl and 10 mM imidazole). The suspension was sonicated at 273 K using an ultrasonic disruptor (UD-211, Takara Tomy) and centrifugation. The supernatant was then subjected to a series of filtration processes at 0.45 μm and 0.22 μm, respectively. The resulting supernatant was purified by immobilized metal affinity chromatography using Nuvia IMAC resin (Bio-Rad). The proteins were eluted with an imidazole concentration gradient (10–400 mM), and the SAL fractions were collected and dialyzed in buffer (0.2 M NaCl, 10 mM MES, pH 6.5) to remove imidazole. Subsequently, the sample was further purified through SP (Toyopearl) column chromatography. The purified protein was loaded onto the column and eluted with a NaCl concentration gradient (0.2–1.0 M). The SAL protein fractions were combined and dialyzed in 0.2 M NaCl, 10 mM MES, pH 6.0. Subsequently, the dialyzed SAL solution was subjected to MonoQ column chromatography (GE Healthcare) to remove extraneous material, and the flow-through fraction was collected as the final purified protein[14,26,37]. The purity of the protein fractions was evaluated using SDS-PAGE electrophoresis.

Measurement of IC_{50} half-inhibition values

Enzyme activity was quantified by measuring the absorbance at 405 nm, which indicates degradation of the *p*-nitrophenylbutyrate (pNPB) ester substrate, as previously reported[14,26,37]. The concentrations of SAL and *p*NPB were adjusted to 0.002 mM and 0.08 mM, respectively. Each assay was conducted in a 1-mL cuvette containing 50 mM HEPES (pH 7.5) and 10% DMSO at 25 °C. To determine the IC_{50} value, a series of inhibitor concentrations (0–1 mM) was prepared. Before initiating the SAL/*p*NPB reaction, SAL was incubated with the inhibitor at 25 °C for 10 min.

Subsequently, the substrate was added, and the increase in the absorbance of free *p*-nitrophenol was monitored at 405 nm. The relative specific activity of SAL was calculated from the slope of the graph for each condition. Inhibition experiments were conducted by adjusting the solution to concentrations that inhibited SAL activity by more or less than 50%. At least three measurements were taken for each experiment, and the mean data for each concentration were used to calculate the IC_{50} value.

Crystallization on the ground and in space

The protein solution was subjected to ultrafiltration using a Vivaspin15 device, resulting in a 30 mg/mL concentration. This solution was then employed in crystallization experiments.

The protein concentration values were determined using the Bio-Rad protein assay kit (Bio-Rad Laboratories, Hercules, CA, USA), with γ-globulin as the standard protein.

The inhibitors were dissolved in DMSO or buffer, added to concentrated SAL, and incubated at 4 °C overnight. The concentrations of the various inhibitors were adjusted to achieve molar concentrations that were 5 to 10 times greater than that of SAL.

The sitting drop vapor diffusion method was conducted at 295 K using a Cryschem plate. A total of 500 μL of the crystallization solution (reservoir) was added to the bottom of the plate, and 2 μL of the mixture of crystallization solution and protein solution was dispensed into the reservoir from the top. Subsequently, the reservoir was sealed.

Experiments to investigate the formation of protein crystals of the highest quality (PCG) have commenced at 293 K. Protein samples and other crystallization apparatus were transported to the International Space Station (ISS) aboard the U.S. SpaceX Dragon resupply ships (SpX-26 and SpX-28). There, astronauts conducted crystallization experiments in the thermostatic chambers of the Kibo laboratory from November to December 2022 and June to July 2023.

The counter-diffusion method represents a specific instance of the broader category of liquid–liquid diffusion methods[29]. The current JAXA PCG employs a silicon tube filled with agarose gel connected to a glass capillary filled with protein solution as the fundamental unit. The crystallization solution diffuses into the capillary through the gel tube, while the protein and other solutes in the capillary diffuse out of the capillary through the gel tube. This bidirectional diffusion allows for the simultaneous exploration of a wide range of crystallization conditions. The ratio of components was modified to (protein, penfluridol, crystallization solution) = 20:1:20. A volume of 12.5 μL per milliliter of crystallization solution and gel immersion solution was administered with the penfluridol and transported to the site.

Data collection, structure determination, and refinement

X-ray diffraction data were collected at SPring-8 beamlines BL41XU and BL44XU at 100 K in a nitrogen stream using a mother solution containing 30% glycerol as a cryoprotectant. The X-ray wavelength was adjusted to 0.9 Å, and the oscillation angle were set to 0.1°, resulting in 180°–360° images. The distance between the crystal and the detector were 240–300 mm. The diffraction images were integrated and scaled using the XDS program package[39] with the *KAMO* automated programming system[40] at SPring-8. The data set was obtained at the limit of resolution where the CC 1/2 value was approximately 0.5[41].

The molecular replacement method, as utilized by the *Phaser* program in the *CCP4* package, was employed to determine the structure[30,31]. The previously reported native structure of SAL (PDB ID: 6KSI) was used as the

search model[14]. The *COOT* program was used to construct the inhibitor molecule and fit the molecular model, and *REFMAC5* was used to refine the structure[32,33].

To fit the model to the electron density map, the inhibitor molecule was constructed with *Coot*'s Ligand builder[32]. Real-space refinement was then employed and continued until convergence using *Refmac* software[33].

Data availability

The structural data supporting the results of this study have been deposited in the Protein Data Bank with the accession codes 9L3C and 9L3S. PDB DOI: https://doi.org/10.2210/pdb9l3s/pdb PDB DOI: https://doi.org/10.2210/pdb9l3c/pdb. All data supporting the findings of this study are available in the paper, as well as its supporting information. Additional requests can be obtained from the corresponding author: kengo@kit.ac.jp.

Received: 9 January 2025; Accepted: 18 March 2025
Published online: 14 April 2025

References

1. Charlotte, S. H. et al. Antimicrobial resistance: a concise update. *Lancet Microbe*. **2025**, 100947. https://doi.org/10.1016/j.lanmic.2024.07.010 (2024).
2. GBD 2021 Antimicrobial Resistance Collaborators. Global burden of bacterial antimicrobial resistance 1990–2021: a systematic analysis with forecasts to 2050. *Lancet* **404**(10459), 1199–1226. https://doi.org/10.1016/S0140-6736(24)01867-1 (2024).
3. Lakhundi, S. & Zhang, K. Methicillin-resistant *Staphylococcus aureus*: molecular characterization, evolution, and epidemiology. *Clin. Microbiol. Rev.* **31**, e00020-18 (2018).
4. Zetola, N., Francis, J. S., Nuermberger, E. L. & Bishai, W. R. Community-acquired methicillin-resistant *Staphylococcus aureus*: an emerging threat. *Lancet Infect. Dis.* **5**, 275–286 (2005).
5. Lowy, F. D. *Staphylococcus aureus* infections. *N. Engl. J. Med.* **339**, 520–532 (1998).
6. Findley, K. & Grice, E. A. The skin microbiome: a focus on pathogens and their association with skin disease. *PLoS Pathog.* **10**, e1004436 (2014).
7. Dinges, M. M., Orwin, P. M. & Schlievert, P. M. Exotoxins of *Staphylococcus aureus*. *Clinic. Microbio. Rev.* **13**, 16–34 (2000).
8. Elena, O., Hikmate, A., Rosario, L. & Antonio, G. Multiple roles of *Staphylococcus aureus* enterotoxins: pathogenicity, superantigenic activity, and correlation to antibiotic resistance. *Toxins (Basel)* **2**, 2117–2131 (2010).
9. Tong, S. Y., Davis, J. S., Eichenberger, E., Holland, T. L. & Fowler, V. G. Jr. *Staphylococcus aureus* infections: epidemiology, pathophysiology, clinical manifestations, and management. *Clin. Microbiol. Rev.* **28**, 603–661. https://doi.org/10.1128/CMR.00134-14.3 (2015).
10. Arciola, C. R., Campoccia, D., Speziale, P., Montanaro, L. & Costerton, J. W. Biofilm formation in *Staphylococcus* implant infections. A review of molecular mechanisms and implications for biofilm-resistant materials. *Biomaterials* **33**, 5967–5982 (2012).
11 Otto, M. Staphylococcal biofilms. *Microbiol. Spectr.* **6**, 4. https://doi.org/10.1128/microbiolspec.GPP3-0023-2018 (2018).
12. Kamitani, S. et al. Induction of neutral lipid-containing granules by staphylococcal lipase from clinical isolates. *SOJ Microbiol. Infect. Dis.* **2**, 1–7 (2015).
13. Kuroda, M., Nagasaki, S., Ito, R. & Ohta, T. Sesquiterpene farnesol as a competitive inhibitor of lipase activity of *Staphylococcus aureus*. *FEMS Microbiol. Lett.* **273**, 28–34 (2007).
14. Kitadokoro, K. et al. Crystal structure of pathogenic *Staphylococcus aureus* lipase complex with the anti-obesity drug orlistat. *Sci. Repo.* **10**, 5469–5469. https://doi.org/10.1038/s41598-020-62427-8 (2020).
15. Heck, A. M., Yanovski, J. A. & Calis, K. A. Orlistat, a new lipase inhibitor for the management of obesity. *Pharmacotherapy* **20**, 270–279. https://doi.org/10.1592/phco.20.4.270.34882 (2000).
16. Sadybekov, A. V. & Katritch, V. Computational approaches streamlining drug discovery. *Nature* **616**, 673–685. https://doi.org/10.1038/s41586-023-05905-z (2023).
17. Friesner, R. A. et al. *Glide*: a new approach for rapid, accurate docking and scoring. 1. Method and assessment of docking accuracy. *J. Med. Chem.* **47**, 1739–1749. https://doi.org/10.1021/jm0306430 (2004).
18. Halgren, T. A. et al. Glide: a new approach for rapid, accurate docking and scoring. 2. Enrichment factors in database screening. *J. Med. Chem.* **47**, 1750–9. https://doi.org/10.1021/jm030644s (2004).
19. Ohashi, H. et al. Potential anti-COVID-19 agents, cepharanthine and nelfinavir, and their usage for combination treatment. *iScience* **24**, 102367. https://doi.org/10.1016/j.isci.2021.102367 (2021).
20. Chong, C. R. & Sullivan, D. J. New uses for old drugs. *Nature* **448**, 645–646. https://doi.org/10.1038/448645a (2007).
21. Ashburn, T. T. & Thor, K. B. Drug repositioning: identifying and developing new uses for existing drugs. *Nat. Rev. Drug Discov.* **3**, 673–683. https://doi.org/10.1038/nrd1468 (2004).
22. Moutselos, K., Kanaris, I., Chatziioannou, A., Maglogiannis, I. & Kolisis, F. N. KEGGconverter: a tool for the in-silico modelling of metabolic networks of the KEGG pathways database. *BMC Bioinform.* **10**, 324. https://doi.org/10.1186/1471-2105-10-324 (2009).
23. Kanehisa, M., Furumichi, M., Sato, Y., Matsuura, Y. & Ishiguro-Watanabe, M. KEGG: biological systems database as a model of the real world. *Nucleic Acids Res.* **53**, D672–D677. https://doi.org/10.1093/nar/gkae909 (2025).
24. Jus, A. et al. Penfluridol: a long-acting oral neuroleptic as therapeutic agent in chronic schizophrenia. *Curr. Ther. Res. Clin. Exp.* **16**, 1041–1058 (1974).
25. van Praag, H. M., Schut, T., Dols, L. & van Schilfgaarden, R. Controlled trial of penfluridol in acute psychosis. *Br. Med. J.* **4**, 710–713. https://doi.org/10.1136/bmj.4.5789.710 (1971).
26. Kitadokoro, J. et al. Crystal structure of *Staphylococcus aureus* lipase complex with unsaturated petroselinic acid. *FEBS Open Bio* **14**, 942–954. https://doi.org/10.1002/2211-5463.13808 (2024).
27. Wedzicha, J. A. et al. Indacaterol-glycopyrronium versus salmeterol-fluticasone for COPD. *N. Engl. J. Med.* **374**, 2222–2234. https://doi.org/10.1056/NEJMoa1516385 (2016).
28. Robson, M. et al. Olaparib for metastatic breast cancer in patients with a germline BRCA mutation. *N. Engl. J. Med.* **377**, 523–533. https://doi.org/10.1056/NEJMoa1706450 (2017).
29. Tanaka, H. et al. A simplified counter diffusion method combined with a 1D simulation program for optimizing crystallization conditions. *J. Synchrotron. Rad.* **11**, 45–48 (2004).
30. McCoy, A. J. et al. *Phaser* crystallographic software. *J. Appl. Crystallogr.* **40**, 658–67429 (2007).
31. Winn, M. D. et al. Overview of the *CCP4* suite and current developments. *Acta Crystallogr. D Biol. Crystallogr.* **67**, 235–242 (2011).
32. Emsley, P., Lohkamp, B., Scott, W. G. & Cowtan, K. Features and development of *Coot*. *Acta Crystallogr. D Biol. Crystallogr.* **66**, 486–501 (2010).
33. Murshudov, G. N. et al. *REFMAC5* for the refinement of macromolecular crystal structures. *Acta. Crystallogr. D Biol. Crystallogr.* **67**, 355–367 (2011).
34. Nardini, M. & Dijkstra, B. W. Alpha/beta hydrolase fold enzymes: the family keeps growing. *Curr. Opin. Struct. Biol.* **9**, 732–737 (1999).

35. Liu, Y. et al. Antimicrobial, antibiofilm, and anti-persister activities of penfluridol against *Staphylococcus aureus*. *Front. Microbiol.* **12**, 727692. https://doi.org/10.3389/fmicb.2021.727692.eCollection (2021).
36. Smyj, R., Wang, X. P. & Han, F. Pimozide. *Profiles Drug Subst. Excip. Relat. Methodol.* **37**, 287–311. https://doi.org/10.1016/B978-0-12-397220-0.00007-6 (2012).
37. Tanaka, M., Kamitani, S. & Kitadokoro, K. *Staphylococcus aureus* lipase: purification, kinetic characterization, crystallization and crystallographic study. *Acta Crystallogr. F Struct. Biol. Commun.* **74**, 567–570 (2018).
38. Bowers, G. N. Jr., McComb, R. B., Christensen, R. G. & Schaffer, R. High-purity 4-nitrophenol: purification, characterization, and specifications for use as a spectrophotometric reference material. *Clin. Chem.* **26**, 724–729 (1980).
39. Kabsch, W. Integration, scaling, space-group assignment and post-refinement. *Acta Crystallogr. D Biol. Crystallogr.* **66**, 125–132 (2010).
40. Yamashita, K., Hirata, K. & Yamamoto, M. *KAMO*: towards automated data processing for microcrystals. *Acta Crystallogr. D Biol. Crystallogr.* **74**, 441–449 (2018).
41. Karplus, P. A. & Diederichs, K. Linking crystallographic model and data quality. *Science* **336**, 1030–1033 (2012).
42. Laskowski, R. A. & Swindells, M. B. *LigPlot+*: multiple ligand-protein interaction diagrams for drug discovery. *J. Chem. Inf. Model.* **51**, 2778–2786 (2011).

Acknowledgements

We are grateful to all members of beamlines BL41XU and BL44XU at SPring-8 for their help in data collection. We thank Profs. Eiki Yamashita and Atsushi Nakagawa of SPring-8 BL44XU for their help with the X-ray data collection. We thank Drs. Kazuya Hasegawa and Seiki Baba of SPring-8 BL41XU, thank you for your help with the X-ray data collection and processing. The use of the synchrotron beamline BL44XU at SPring-8 was obtained through the Cooperative Research Program of the Institute for Protein Research, Osaka University (proposal numbers 2019A6912, 2019B6912, 2020A6512, 2020B6512, 2021A6611, 2021B6611,6908 2022A6710, 2022B6710, 2023A6809, 2023A6809 and 2024A6908). This research was supported [in part] by the Basis for Supporting Innovative Drug Discovery and Life Science Research (BINDS) Platform Project from AMED under grant numbers JP21am010170, JP21am0101072, JP21am0101092, and JP21am0101114. This research formed part of the "High-Quality Protein Crystal Growth Experiment on KIBO" administered by JAXA. American Spacecraft "Space X Dragon" was used for space transportation. Some of the space crystallization technology was developed by the European Space Agency and the University of Granada. We would like to thank the Kanehisa Laboratory for giving us permission to use the KEGG database. We would also like to thank the staff at Space BD for all of their help and support.

Author contributions

KK, TH, KI, KM, and SK designed the research. JK, TH, MK, NF, YO, TH, MY, KI, KM, SK, and KK performed the research. JK, TH, MK, NF, YO, TH, MY, KI, KM, SK, and KK analyzed the data. JK, TH, KK, and SK coordinated the work and drafted the manuscript.

Funding

This work was partly supported by Grants-in-Aid for Scientific Research from the Japanese Ministry of Education, Culture, Science, and Technology (24K10199).

Competing interests

The authors declare no competing interests.

Additional information

Supplementary Information The online version contains supplementary material available at https://doi.org/10.1038/s41598-025-94981-4.

Correspondence and requests for materials should be addressed to K.K.